2015

Traveling Waves and their Tails in Locally Resonant Granular Systems

H Xu
University of Massachusetts Amherst, haitao@math.umass.edu

P G. Kevrekidis
University of Massachusetts Amherst, kevrekid@gmail.com

A Stefanov
University of Kansas, stefanov@ku.com

Traveling waves and their tails in locally resonant granular systems

2015 J. Phys. A: Math. Theor. 48 195204

(http://iopscience.iop.org/1751-8121/48/19/195204)

IOP Publishing Journal of Physics A: Mathematical and Theoretical
J. Phys. A: Math. Theor. **48** (2015) 195204 (19pp) doi:10.1088/1751-8113/48/19/195204

Traveling waves and their tails in locally resonant granular systems

H Xu[1], P G Kevrekidis[1,2] and A Stefanov[3]

[1] Department of Mathematics and Statistics, University of Massachusetts, Amherst MA 01003-4515, USA
[2] Center for Nonlinear Studies and Theoretical Division, Los Alamos National Laboratory, Los Alamos, NM 87544, US
[3] Department of Mathematics University of Kansas 1460 Jayhawk Blvd Lawrence, KS 66045-7523, US

E-mail: haitao@math.umass.edu, kevrekid@gmail.com and stefanov@ku.com

Received 17 December 2014, revised 13 March 2015
Accepted for publication 16 March 2015
Published 22 April 2015

Abstract

In the present study, we revisit the theme of wave propagation in locally resonant granular crystal systems, also referred to as mass-in-mass systems. We use three distinct approaches to identify relevant traveling waves. The first consists of a direct solution of the traveling wave problem. The second one consists of the solution of the Fourier tranformed variant of the problem, or, more precisely, of its convolution reformulation (upon an inverse Fourier transform) in real space. Finally, our third approach will restrict considerations to a finite domain, utilizing the notion of Fourier series for important technical reasons, namely the avoidance of resonances, which will be discussed in detail. All three approaches can be utilized in either the displacement or the strain formulation. Typical resulting computations in finite domains result in the solitary waves bearing symmetric non-vanishing tails at both ends of the computational domain. Importantly, however, a countably infinite set of anti-resonance conditions is identified for which solutions with genuinely rapidly decaying tails arise.

Keywords: mass in mass, locally resonant, traveling wave, mass with mass, Fourier transform, granular chain

(Some figures may appear in colour only in the online journal)

1. Introduction

The theme of granular chains has gained considerable traction over the past decade, perhaps to a large measure due to the significant advances in corresponding experimental techniques complementing theoretical and numerical investigations [1–4]. While traveling waves in these extensively tunable (regarding, e.g., their homogeneous or heterogeneous, weakly or strongly nonlinear nature) media have received the lion's share of the corresponding attention, numerous other excitations have been examined more recently as well including, but not limited to, defect modes, bright and dark breathers, and shock waves, among others; see e.g. [5–45] for some characteristic examples. A key feature supporting this explosive rate of development has been the versatile use of such settings in a diverse host of applications including e.g., actuating devices [9], acoustic lenses [46], mechanical diodes [47–49], logic gates [50] and sound scramblers [51, 52].

The principal theme of robust, highly localized traveling stress waves in such a setting has received arguably the most attention, as it has posed significant mathematical challenges and has proved fruitful in a diverse array of applications including, among others, e.g. the quantification of bone-quality in biomedical applications [53] or the monitoring of hydration of gypsum cement [54]. From a theoretical perspective, the existence of such waves, originally established in [17] (see also [1]), was rigorously proved in [55] by means of the variational approach of [56]. However, the non-constructive nature of this proof offered no information on the solutions' profile or on their speed dependence on wave amplitude and space scale, unlike [17]. Their single pulse character (in the strain variables of the system) was subsequently established rigorously in [39], following the approach of [43]. These approaches also enabled the identification of the doubly exponential character of their spatial decay in the absence of the so-called precompression (i.e., of linear part within the system dynamics); see also for earlier relevant asymptotic analyses predicting this rate of spatial decay [44, 45].

While this part of the story is admittedly well-understood in the context of the standard one-component, homogeneous granular chain, in recent years, a number of intriguing variants have emerged on this theme which may possess more elaborate structural characteristics as regards their traveling waves (and other related structures). Chronologically, an earlier example of this form consists of the so-called cradle system (of which we are not aware of an experimental realization as of yet) proposed in [57] and further explored, including by detailed direct numerical computations in [58]. There, a local, linear oscillator was added to the granular chain, emulating the pendulum restoring effect in the well-known Newton's cradle. In that context, numerous unexpected features arose including the formation of waves with persistent tails, of traveling (time-periodic) breathers, of apparently direction-reversing (so-called boomeron-type) structures, etc. While many of these observations have yet to be explained, here we will actually turn our attention to another class of systems, the so-called locally resonant granular crystals, otherwise known as mass-in-mass (MiM) or mass-with-mass (MwM) systems.

The MiM and MwM systems are rapidly gaining an increasing amount of interest chiefly because they have already been experimentally realized in [59] and [60], respectively. Admittedly, both of these realizations were chiefly linear (in the presence of externally imposed pre-compression of the chain) and aiming to illustrate the remarkable meta-material type properties that these systems possess. Yet, while a MwM nonlinear prototype was also demonstrated in [61], it was a different type of experiment that very recently realized highly nonlinear propagation in a locally resonant granular system [62]. In particular, the experiment

of [62] built a so-called woodpile configuration consisting of orthogonally stacked rods (every second rod is aligned, in this alternating 0–90 degree configuration) and demonstrated that the internal vibrations of the rods can play the role of the local resonator within the granular chain. It was also shown that depending on the properties of the system (i.e., the length of the rods), one can controllably incorporate one or more such resonators, yet here our focus will be in the case of a single such resonator.

A remarkable find of these locally resonant, highly nonlinear chains was found to be the propagation of traveling waves with an apparently non-decaying tail [62]. It was indeed found that the tail behind the wave may persist in small amplitude oscillations (in the experiment they were found to potentially be three orders of magnitude smaller than the core of the traveling wave) which, however, do not decay and which bear a clear frequency/wavenumber, namely that of the out-of-phase vibration between the principal and the resonating mass in such a system. Weakly nonlocal solitary waves have been studied extensively in a series of examples in physical sciences and engineering [63, 64], yet very few (especially so, highly experimentally controllable) realizations thereof are known to exist. Our aim in the present work is to examine more systematically such traveling waves from a theoretical perspective.

We will use three distinct approaches in order to identify this important class of solutions for the MiM/MwM systems. We will seek them directly as traveling waves in real space, by attempting to identify fixed points of a discretization of the co-traveling frame nonlinear problem in our direct method. We will also follow the approach of [43], rewriting the problem in Fourier space (upon a Fourier transform) and seeking fixed points of that variant upon inverse Fourier transform, similarly to [39, 43]. This will recover a convolution based reformulation of the problem in real space. Finally, the third method will recognize the limitations of the infinite domain formulation of the above convolution problem and will instead restrict consideration to a finite lattice, using Fourier series rather than Fourier transforms. The presentation of the three methods will take place in section 2 below. These methods will be explored in a *finite domain* setting yielding convergence to exact traveling waves under suitable conditions that will be explicitly analyzed. In addition to the, arguably more tractable, pulse-like solutions of the so-called strain variant of the problem, we will also translate the results at the level of bead displacements. Relevant numerical results will be given in section 3 of the manuscript, along with some of the nontrivial associated challenges of the computations and impact of parametric variations on the resulting waves. In that process, a particularly interesting feature will be identified (and subsequently explained), namely for an isolated, countably infinite set of parameters the problem will no longer possess the oscillating tails described above, but rather the symmetric, rapidly decaying tails of the standard granular chain. Finally, in section 4, we will summarize our findings and present some potential directions for future work.

2. Theoretical setup

2.1. Model and traveling wave formulation

Our starting point will consist of a Hertzian chain [1] of identical beads with the displacement of the nth bead from the original position denoted by U_n. For the nth bead ($n = 1, 2, \ldots, N$), we attach a local resonator, effectively coupling it to another kind of bead (the 'MiM' [59] or

the 'MwM' [60] discussed above), whose displacement from the original position is denoted by V_n. Notice that in the case of the woodpile configuration, this does not constitute a separate mass but rather reflects the internal vibrational modes of the woodpile rods [62]. Here we use K_1 to stand for the spring constant; R for the radius of the bead, ρ for the density, E for the elastic modulus, μ for the Poisson's ratio of the bead so that the mass $m_u = \frac{4}{3}\pi\rho R^3$; ν_1 reflects the ratio of two kinds of masses $\frac{m_v}{m_u}$ (or more generally, the effective mass of the locally resonant mode). With these assumptions, we write our model of the MiM/MwM problem as follows:

$$m_u\ddot{U}_n = \frac{4}{3}E_*\sqrt{\frac{R}{2}}\left[\left(\delta_1 + U_{n-1} - U_n\right)_+^p - \left(\delta_1 + U_n - U_{n+1}\right)_+^p\right] - K_1\left(U_n - V_n\right), \tag{1}$$

$$m_v\ddot{V}_n = -K_1\left(V_n - U_n\right). \tag{2}$$

Here $n \in \mathbf{Z}$, and δ_1 is the initial pre-compression between beads, while $p = 3/2$ is determined by the Hertzian interaction and $E_* = \frac{E}{2(1-\mu^2)}$. The plus subscripts mean that the terms in the parentheses will be considered only when their arguments are non-negative and will be set to zero values otherwise.

By defining $k_1 = \frac{3K_1}{2\sqrt{2}E_*R}$, $\delta_0 = \frac{\delta_1}{R}$, $u_n = \frac{U_n}{R}$, $v_n = \frac{V_n}{R}$ and time $t_{\text{new}} = (\sqrt{\frac{1}{2}}\frac{E_*}{\pi\rho R^2})^{\frac{1}{2}}t_{\text{old}}$, we obtain the nondimensional system as:

$$\ddot{u}_n = \left(\delta_0 + u_{n-1} - u_n\right)_+^p - \left(\delta_0 + u_n - u_{n+1}\right)_+^p - k_1(u_n - v_n), \tag{3}$$

$$\nu_1\ddot{v}_n = -k_1(v_n - u_n). \tag{4}$$

Focusing on traveling wave solutions of the above system, we seek them in the form $u_n(t) = r(n - ct) = r(\xi)$ and $v_n(t) = s(n - ct) = s(\xi)$, i.e., going to the co-traveling frame with c as the traveling speed, obtaining advance-delay differential equations for the profile dependence on the co-traveling frame variable ξ:

$$c^2\ddot{r}(\xi) = \left(\delta_0 + r(\xi - 1) - r(\xi)\right)_+^p - \left(\delta_0 + r(\xi) - r(\xi + 1)\right)_+^p - k_1(r(\xi) - s(\xi)), \tag{5}$$

$$c^2\nu_1\ddot{s}(\xi) = -k_1(s(\xi) - r(\xi)). \tag{6}$$

Moreover, if we consider the equations of relative displacements (i.e., the strain variables), writing $R(\xi) = r(\xi - 1) - r(\xi)$ and $S(\xi) = s(\xi - 1) - s(\xi)$, the equations assume the form:

$$c^2\ddot{R}(\xi) = \left(\delta_0 + R(\xi + 1)\right)_+^p + \left(\delta_0 + R(\xi - 1)\right)_+^p - 2\left(\delta_0 + R(\xi)\right)_+^p - k_1(R(\xi) - S(\xi)), \tag{7}$$

$$c^2\nu_1\ddot{S}(\xi) = -k_1(S(\xi) - R(\xi)). \tag{8}$$

The discrete version of the strain equations can be obtained as:

$$\ddot{x}_n(t) = \left(\delta_0 + x_{n+1}\right)_+^p + \left(\delta_0 + x_{n-1}\right)_+^p - 2\left(\delta_0 + x_n\right)_+^p - k_1(x_n - y_n), \tag{9}$$

$$\nu_1\ddot{y}_n(t) = -k_1(y_n - x_n), \tag{10}$$

where $x_n(t) = u_{n-1} - u_n$ and $y_n(t) = v_{n-1} - v_n$.

Remark 1. If $r(\xi)$ and $s(\xi)$ are solutions to equations (5)–(6) with current parameters, $\tilde{r} = a^4 r$ and $\tilde{s} = a^4 s$ will solve those equations with $\tilde{c} = ac$, $\tilde{k}_1 = a^2 k_1$ and $\tilde{\delta}_0 = a^4\delta_0$.

Similarly, there is a family of solutions to equations (7)–(8) with different speeds, amplitudes and other parameters.

Our first solution method of this system will consist of a direct method attempt at solving this problem at the level of equations (5)–(6) for the displacements or of equations (7)–(8) for the strains in real space. This approach is denoted by 'scheme I' in what follows.

2.2. Infinite domain with Fourier transform

In this subsection, we consider the infinite domain situation, where $\xi \in (-\infty, \infty)$, bearing in mind, however, that in realistic setups this is practically irrelevant, as all numerical computations and experimental observations are conducted in finite domain settings. Additionally, our analysis will be restricted to the highly nonlinear regime whereby $\delta_0 = 0$.

Here we assume R and S are functions such that Fourier transform $\hat{f}(k) = \int_{-\infty}^{\infty} f(\xi) e^{-ik\xi} d\xi$ can be applied on R, S, $\ddot{R}$, $\ddot{S}$ and $(R^{3/2})_+$. This condition is necessary because the above-mentioned experimental observations [62] suggest that $R(\xi)$ and $S(\xi)$ sometimes bear non-decaying (yet bounded) oscillating tails as $|\xi| \to \infty$. This implies that R and S may be non-integrable and thus their Fourier transforms may not be possible to define. In this subsection we will only focus on the special cases for R and S where such integrable solutions do exist.

With the assumption above, we apply Fourier transform to equations (7)–(8) to obtain:

$$\left(k_1 + k_1\nu_1 - c^2\nu_1 k^2\right)\hat{R} = \frac{1}{c^2}\left(k_1 - c^2\nu_1 k^2\right)\mathrm{sinc}^2\left(\frac{k}{2}\right)\widehat{\left(R^{3/2}\right)_+}, \tag{11}$$

$$\left(k_1 - c^2\nu_1 k^2\right)\hat{S} = k_1\hat{R} \tag{12}$$

with $\mathrm{sinc}(k)$ being defined as $\frac{\sin(k)}{k}$. If $\hat{R}$, $\hat{S}$ and $\widehat{(R^{3/2})_+}$ are well-defined functions, the following conditions should be satisfied:

(a) $\hat{R}(\pm\sqrt{\frac{k_1}{c^2\nu_1}}) \equiv \hat{R}(\pm k_2) = 0$;

(b) $\widehat{(R^{3/2})_+}(\pm\sqrt{\frac{k_1(1+\nu_1)}{c^2\nu_1}}) \equiv \widehat{(R^{3/2})_+}(\pm k_0) = 0$ or $k_0 = 2n\pi$.

Here we defined $k_0 = \sqrt{\frac{k_1(1+\nu_1)}{c^2\nu_1}}$ and $k_2 = \sqrt{\frac{k_1}{c^2\nu_1}}$.

If we choose $k_0 = 2n\pi$, the condition (b) is automatically met and the zeros of $\hat{R}$ will be investigated later for the condition (a). In this case, the second one among equations (11) and (12) can be directly solved and back-substituted in the first, to yield $\hat{R} = \frac{k_1 - c^2\nu_1 k^2}{c^2(k_1 + k_1\nu_1 - c^2\nu_1 k^2)}\mathrm{sinc}^2(\frac{k}{2})\,\widehat{(R^{3/2})_+} \equiv M_1(k)\,\widehat{(R^{3/2})_+}$. Since $\lim_{k\to\pm k_0}\frac{\mathrm{sinc}^2(\frac{k}{2})}{k^2 - k_0^2} = 0$, the singularities of $M_1(k)$ at $\pm k_0$ can be removed when $k_o = 2n\pi$. Moreover, if we define the inverse Fourier transform of $\hat{f}(k)$ as $f(\xi) = \frac{1}{2\pi}\int_{-\infty}^{\infty}\hat{f}(k)e^{ik\xi}dk$, then the inverse Fourier transform of $M_1(k)$ is

$$
\begin{aligned}
m_1(\xi) &= \mathcal{F}^{-1}\left[\frac{1}{c^2}\left(1+\frac{k_1}{c^2}\frac{1}{k^2-k_0^2}\right)\mathrm{sinc}^2\left(\frac{k}{2}\right)\right] \\
&= \frac{1}{c^2}\mathcal{F}^{-1}\left[\frac{\sin^2\left(\frac{k}{2}\right)}{\left(\frac{k}{2}\right)^2}\left(1-\frac{k_1}{c^2k_0^2}\right)+\frac{k_1}{c^2k_0^2}\frac{\sin^2\left(\frac{k}{2}\right)}{\left(\frac{k^2-k_0^2}{4}\right)}\right] \\
&= \frac{1}{c^2}\left(1-\frac{k_1}{c^2k_0^2}\right)\mathcal{F}^{-1}\left[\frac{\sin^2\left(\frac{k}{2}\right)}{\left(\frac{k}{2}\right)^2}\right]+\frac{k_1}{c^4k_0^2}\mathcal{F}^{-1}\left[\frac{\sin\left(\frac{k-k_0}{2}\right)}{\left(\frac{k-k_0}{2}\right)}\frac{\sin\left(\frac{k+k_0}{2}\right)}{\left(\frac{k+k_0}{2}\right)}\right] \\
&= \frac{1}{c^2}\left(1-\frac{k_1}{c^2k_0^2}\right)(1-|\xi|)I_{[-1,1]}(\xi)+\frac{k_1}{c^4k_0^2}\left[\left(\mathrm{e}^{\mathrm{i}k_0\xi}I_{[-\frac{1}{2},\frac{1}{2}]}(\xi)\right)*\left(\mathrm{e}^{-\mathrm{i}k_0\xi}I_{[-\frac{1}{2},\frac{1}{2}]}(\xi)\right)\right] \\
&= \frac{1}{c^4k_0^2}\left[\left(c^2k_0^2-k_1\right)(1-|\xi|)-\frac{k_1}{k_0}\,\mathrm{sgn}(\xi)\sin\left(k_0\xi\right)\right]I_{[-1,1]}(\xi) \qquad (13)
\end{aligned}
$$

by direct calculation, where $I_{[a,b]}$ has been used to denote the indicator function in the corresponding interval. Utilizing the convolution theorem, equation (11) can be transformed back to real space as:

$$R(\xi) = \left(m_1 * \left(R^{3/2}\right)_+\right)(\xi), \qquad (14)$$

where $*$ will be used hereafter to denote the convolution.

Then, by iterating $R^{(l)} \to ((R^{3/2})_+)^{(l)} \to R^{(l+1)}$ using equation (14), in the same spirit as the calculation of [43] (see also the much earlier similar proposal of [65]), we obtain yet a new scheme, hereafter termed 'scheme II'.

Next, we will try to find $S(\xi)$ from equation (12). Theoretically, one can follow the order $R \to \hat{R} \to \hat{S} \to S$ to find $S(\xi)$. But the singularity points of $\hat{S}$ can induce practical difficulties in this vein of numerical computations. Instead, we use the relationship between $\hat{S}$ and $\widehat{(R^{3/2})_+}$

$$\hat{S} = -\frac{k_1}{c^4\nu_1\left(k^2-k_0^2\right)}\mathrm{sinc}^2\left(\frac{k}{2}\right)\widehat{\left(R^{3/2}\right)_+} \equiv M_2(k)\,\widehat{\left(R^{3/2}\right)_+} \qquad (15)$$

to reach $S(\xi)$ since $\widehat{(R^{3/2})_+}$ is already known. Similar to deriving equation (14), we find the inverse Fourier transform of $M_2(k)$ as

$$
\begin{aligned}
m_2(\xi) &= \mathcal{F}^{-1}\left[-\frac{k_1}{c^4\nu_1\left(k^2-k_0^2\right)}\mathrm{sinc}^2\left(\frac{k}{2}\right)\right] \\
&= \frac{k_1}{c^4\nu_1k_0^2}\mathcal{F}^{-1}\left[\frac{\sin^2\left(\frac{k}{2}\right)}{\left(\frac{k}{2}\right)^2}-\frac{\sin^2\left(\frac{k}{2}\right)}{\left(\frac{k^2-k_0^2}{4}\right)}\right]
\end{aligned}
$$

$$= \frac{k_1}{c^4\nu_1 k_0^3}\left[k_0(1-|\xi|)+\mathrm{sgn}(\xi)\sin\left(k_0\xi\right)\right]I_{[-1,1]}(\xi) \tag{16}$$

and apply the convolution theorem again on equation (15), to obtain

$$S(\xi) = \left(\left(m_2 * R^{3/2}\right)_+\right)(\xi). \tag{17}$$

It is noticed that functions m_1 and m_2 have explicit expressions with finite support $(-1, 1)$ derived in equations (13) and (16) when we set $k_0 = 2n\pi$. As a result, R and S that we obtained from the integration equations are smooth, localized and integrable functions and Fourier transform on these functions will be applicable once the parameters are chosen such that $\sqrt{\frac{k_1(1+\nu_1)}{c^2\nu_1}} = 2n\pi$. Illustrations of the solution of R and S solved from equations (14)–(17) with numerical evidence will be shown in section 3. On the other hand, setting $\frac{k_0}{2\pi} \notin \mathbb{Z}$ will bring about not only difficulties in finding the values of $\hat{R}(\pm k_0)$ through the iterative method but also failure to derive the convolution equations (14)–(17) via inverse Fourier transform. Later, an alternative scheme will be introduced to solve the system not satisfying $\frac{k_0}{2\pi} \in \mathbb{Z}$ and the results will show that the non-decaying oscillatory tails are present in the solution of R and S, which implies that only under condition $k_0 = 2n\pi$ the oscillation tails can be removed. In the observations of experiments or simulations (where k_1 and ν_1 are known from the settings), the traveling-wave solutions without oscillatory tails will be expected to exist with velocities $c = \frac{\sqrt{k_1(1+1/\nu_1)}}{2n\pi}$, where $n \in \mathbb{Z}$.

From a physical perspective, the anti-resonance condition $k_0 = 2n\pi$ appears to signal a matching between wavenumbers enabling translation of the energy within the underlying granular lattice and the internal vibration wavenumber/frequency of each resonator such that the energy can fully be transferred from one lattice site to the next and hence a genuine traveling wave can be produced. On the other hand, when this condition is not satisfied some energy will be retained within each resonator, oscillators producing a non-vanishing tail for the wave.

2.3. Finite domain with Fourier series

As a result of the necessity to explore realistic computations and observations, it is natural to also consider the problem as restricted on a finite domain, i.e., for $\xi \in [-L, L]$. Then, we will express the corresponding functions as Fourier series instead of using their Fourier transforms. In this case, the bounded nature of our profiles, in conjunction with the finiteness of the domains guarantees integrability. R, S and R_+^p can then be expressed in the form of Fourier series $f(\xi) = \sum_{k=-\infty}^{\infty} f_k \mathrm{e}^{\mathrm{i}\frac{2\pi}{2L}k\xi}$, where $f_k = \frac{1}{2L}\int_{-L}^{L} f(\xi)\mathrm{e}^{-\mathrm{i}\frac{2\pi}{2L}k\xi}\mathrm{d}\xi$. It can be shown when $f(\xi)$ is (piecewise) smooth in the interval $[-L, L]$, then its Fourier series will converge to f in $[-L, L]$. Since this condition is not difficult to achieve, we assume R, S and R_+^p are such functions. Then equations (7) and (8) can be written as:

$$\left(k_1 + k_1\nu_1 - c^2\nu_1\left(\frac{\pi}{L}k\right)^2\right)R_k = \frac{1}{c^2}\left(k_1 - c^2\nu_1\left(\frac{\pi}{L}k\right)^2\right)\mathrm{sinc}^2\left(\frac{\pi}{2L}k\right)\left(R_+^{3/2}\right)_k, \tag{18}$$

$$\left(k_1 - c^2\nu_1\left(\frac{\pi}{L}k\right)^2\right)S_k = k_1 R_k, \tag{19}$$

where $k \in \mathbb{Z}$.

It is straightforward to observe that equations (18) and (19) are just discrete versions of equations (11) and (12). However, the fact that k only assumes integer values can greatly facilitate the avoidance of singularities in these equations and hence the unobstructed performance of the relevant computations. Nevertheless, there are still requirements on R_k and $((R^{3/2})_+)_k$ so that equations (18) and (19) can be defined for any integer k:

(c) If $\sqrt{\frac{k_1(1+1/\nu_1)L^2}{c^2\pi^2}} = k_0\frac{L}{\pi} \in \mathbb{Z}$ and $k_0 \neq 2nL$, $((R^{3/2})_+)_{k_0\frac{L}{\pi}} = ((R^{3/2})_+)_{-k_0\frac{L}{\pi}} = 0$;

(d) If $\sqrt{\frac{k_1L^2}{c^2\nu_1\pi^2}} = k_2\frac{L}{\pi} \in \mathbb{Z}$, $((R^{3/2})_+)_{k_2\frac{L}{\pi}} = ((R^{3/2})_+)_{-k_2\frac{L}{\pi}} = 0$.

If we assume $k_0\frac{L}{\pi} \notin \mathbb{Z}$, then conditions (c)-(d) will not be violated and equation (18) can be expressed as $R_k = \frac{(k_1 - c^2\nu_1(\frac{\pi}{L}k)^2)}{c^2(k_1+k_1\nu_1-c^2\nu_1(\frac{\pi}{L}k)^2)}\mathrm{sinc}^2(\frac{\pi}{2L}k)(R_+^{3/2})_k = \tilde{M}_{1_k}(R_+^{3/2})_k$. Since $\tilde{m}_1(\xi) = \sum_{k=-\infty}^{\infty}\tilde{M}_{1_k}\mathrm{e}^{\mathrm{i}\frac{2\pi}{2L}k\xi}$ converges and $\frac{1}{2L}\int_{-L}^{L} f_j\,\mathrm{e}^{\mathrm{i}j\frac{2\pi}{2L}y}g_k\mathrm{e}^{\mathrm{i}k\frac{2\pi}{2L}(\xi-y)}\mathrm{d}y = f_j\,g_k\mathrm{e}^{\mathrm{i}k\frac{2\pi}{2L}\xi}\delta_{jk}$, the equation $R_k = \tilde{M}_{1_k}(R_+^{3/2})_k$ can be rewritten using convolution as:

$$R(\xi) = \frac{1}{2L}\left(\tilde{m}_1 * \left(R^{3/2}\right)_+\right)(\xi), \tag{20}$$

where in this case the convolution is restricted to the domain $[-L, L]$.

In order to get S, we define $\tilde{m}_2(\xi) = \sum_{k=-\infty}^{\infty}\frac{k_1}{c^2(k_1+k_1\nu_1-c^2\nu_1(\frac{\pi}{L}k)^2)}\mathrm{sinc}^2(\frac{\pi}{2L}k)\mathrm{e}^{\mathrm{i}\frac{2\pi}{2L}k\xi} = \sum_{k=-\infty}^{\infty}\tilde{M}_{2_k}\mathrm{e}^{\mathrm{i}\frac{2\pi}{2L}k\xi}$ and similarly obtain the equation:

$$S(\xi) = \frac{1}{2L}\left(\tilde{m}_2 * \left(R^{3/2}\right)_+\right)(\xi). \tag{21}$$

Again, the convolution in the equation is only defined within $[-L, L]$. The above setting realizes a way of finding $R(\xi)$ and $S(\xi)$ on a finite domain which will hereafter be denoted as 'scheme III'. Being different from 'scheme II', this scheme is able to deal with the situation where the traveling-wave solution has non-decaying oscillatory tails, namely, when $\frac{k_0}{2\pi} \notin \mathbb{Z}$. But we should also bear in mind that this new scheme is only numerically implementable when $k_0\frac{L}{\pi} \notin \mathbb{Z}$ due to the singularities of $\tilde{M}_{1_k}$ and $\tilde{M}_{2_k}$. From a physical perspective, for a solution to exist in the finite domain, and for the 'storing' of energy to occur in its tails, the above condition suggests that the resonator's vibrational wavenumber should not coincide with one of the (quantized, for the finite domain) wavenumbers accessible to the lattice. However, we should point out here that these physical interpretations (this finite domain one, as well as the one for the important anti-resonance scenario) may be worthwhile subjects for further investigation.

3. Numerical results of schemes

3.1. Discussion about schemes II and III

Scheme I does not involve any extra assumptions, aside from the proposed existence of traveling waves. Our numerical implementation of this scheme also employs a discretization to identify the relevant structure by means of a fixed point iterative solution of the associated boundary value problem. Thus, it appears to be the one with the least amount of additional assumptions (cf the discussions above) and as such perhaps the one most likely to converge to the desired solutions. However, a complication here involves the potentially non-vanishing boundary conditions on a finite domain and the identification, *a priori*, of a suitable initial guess that may properly capture the behavior at $\xi \to \pm\infty$.

Scheme II, as indicated above, is appropriate only with the anti-resonance condition $k_0 = 2n\pi$. Under this condition, we start the algorithm with a triangle function and find it to converge to a solution of R without oscillating tails. Other properties and condition $\hat{R}(\pm k_2) = 0$ can be easily verified on the numerical solution of R then.

It is worth noting that although this scheme is derived in the infinite domain setting, all the computations associated with it will be realized, by necessity, on finite domains.

In scheme III, k_0 can assume any value except for ones such that $k_0\frac{L}{\pi} \in \mathbb{Z}$. Since the effect of the domain size on the solution is considered here and L is involved explicitly in the equations, we can always adjust L to make $k_0\frac{L}{\pi} \notin \mathbb{Z}$, whatever the values of ν_1, k_1 and c are. It should be noticed that we can vary L (except $k_0\frac{L}{\pi} \in \mathbb{Z}$) while keeping all other parameters fixed to obtain a family of solutions of $R(\xi)$ and $S(\xi)$ to equation (20) and (21). The study of the solutions as a family would be an interesting direction itself and we'll report our further investigation in the future.

With $\frac{k_0}{2\pi} \in \mathbb{Z}$ and $\frac{k_0 L}{\pi} \notin \mathbb{Z}$, there are cases that can be calculated with both schemes II and III. As numerical results suggest, these two schemes end up with the same solution when k_0 is eligible for both of them, naturally demonstrating a strong connection between the two different approaches, which can be explained by the relationship between Fourier transform and Fourier series. We note that when a function $f(\xi)$ has compact support $[-L, L]$, the coefficients f_k of its Fourier series (periodic extension with period $2L$) are related to the Fourier transform of that function $\hat{f}(k)$ evaluated at certain points, i.e. $f_k = \frac{\hat{f}(\frac{k\pi}{L})}{2L}$. Thus it can be shown that $m_1(\xi) = \sum_{k=-\infty}^{\infty}(\frac{1}{2L}\int_{-L}^{L} m_1(y)\mathrm{e}^{-\mathrm{i}\frac{2\pi}{2L}ky}\mathrm{d}y)\mathrm{e}^{\mathrm{i}\frac{2\pi}{2L}k\xi} = \sum_{k=-\infty}^{\infty}\frac{1}{2L}M_1(k\frac{\pi}{L})\mathrm{e}^{\mathrm{i}\frac{2\pi}{2L}k\xi} = \sum_{k=-\infty}^{\infty}\frac{1}{2L}\tilde{M}_{1k}\mathrm{e}^{\mathrm{i}\frac{2\pi}{2L}k\xi}$ $= \frac{1}{2L}\tilde{m}_1(\xi)$, implying equations (14) and (20) are two equivalent formulations when both are applicable. Similar arguments can be applied to show the connection between $m_2 = \frac{1}{2L}\tilde{m}_2$ and the equivalence of equations (15) and (21) under the same conditions about L and k_0.

Besides the anti-resonance situation $\frac{k_0}{2\pi} \in \mathbb{Z}$, direct calculation also reveals that

$$
\begin{aligned}
&\frac{1}{2L}\tilde{m}_1(\xi)\\
&= \frac{1}{2L}\sum_{k=-\infty}^{\infty}\frac{1}{c^2}\left(1 + \frac{k_1}{c^2}\frac{1}{\left(k\frac{\pi}{L}\right)^2 - k_0^2}\right)\mathrm{sinc}^2\left(\frac{k\pi}{2L}\right)\mathrm{e}^{\mathrm{i}\frac{2\pi}{2L}k\xi}\\
&= \frac{1}{2L}\sum_{k=-\infty}^{\infty}\left[\left(\frac{1}{c^2} - \frac{k_1}{k_0^2c^4}\right)\mathrm{sinc}^2\left(\frac{k\pi}{2L}\right) - 2\frac{k_1}{k_0^2c^4}\frac{1}{\left(k\frac{\pi}{L}\right)^2 - k_0^2}\left(\cos\left(\frac{k\pi}{L}\right) - 1\right.\right.\\
&\qquad \left.\left. + (1 - \cos(k))\cos\big(k_0L + k\pi\big)\right)\right]\mathrm{e}^{\mathrm{i}\frac{2\pi}{2L}k\xi}\\
&= \frac{1}{2k_0^2c^4}\Big[2\big(c^2k_0^2 - k_1\big)\max(1 - |x|, 0)\\
&\qquad + k_1\big(-2|x|\,\mathrm{sinc}\big(k_0x\big) + |x+1|\,\mathrm{sinc}\big(k_0(x+1)\big)\\
&\qquad + |1-x|\,\mathrm{sinc}\big(k_0(1-x)\big)\big)\Big]\\
&:= \bar{m}_1(\xi)
\end{aligned}
\tag{22}
$$

holds when $k_0\frac{L}{\pi}+\frac{1}{2}\in\mathbb{Z}$. Similarly it can be shown that $\frac{1}{2L}\tilde{m}_2(\xi)=\frac{k_1}{2\nu_1 k_0^2 c^4}[2\max(1-|x|,0)+2|x|\,\mathrm{sinc}(k_0x)-|x+1|\,\mathrm{sinc}(k_0(x+1))-|1-x|\,\mathrm{sinc}(k_0(1-x)))]\coloneqq\bar{m}_2(\xi)$ under the same condition. However, there does not exist any explicit function form for the limit of $\tilde{m}_i(i=1,2)$ as $L\to\infty$ since $\tilde{m}_i$ will encounter singularity points at $L=\frac{n\pi}{k_0}$, where $n\in\mathbb{Z}$.

Thanks to the use of the convolution theorem, implementation of schemes II and III has become straightforward, provided the respective constraint conditions discussed above are applicable.

If so, our numerical computations of scheme III indicate that the oscillating tails are generically present when $\frac{k_0}{2\pi}\notin\mathbb{Z}$, as shown in figure 1. While if $k_0=2n\pi$, $n\in\mathbb{Z}$, as in the case of figure 2 (including also computations from scheme I), the nondecaying oscillatory tails are absent. For a better view of the classification of different anti-resonance/resonance situations and corresponding results, please see table 1. Later in the subsection C, we discuss more about these schemes and their numerical results as functions of the system's parameters.

3.2. Further discussion about scheme I

Scheme III discussed above represents the most direct way of obtaining a numerically exact (up to a prescribed tolerance) solution to the traveling wave problem, and typically it constitutes our most direct technique, as illustrated e.g. in figures 1–2. Additionally, however, a few iterations of this Scheme could be used to provide us with a good initial guess for attacking the problem by means of the more direct equations (5)–(6) or equations (7)–(8). In that vein, we find that upon defining $f=-c^2\ddot{R}(\xi)+(\delta_0+R(\xi+1))_+^p+(\delta_0+R(\xi-1))_+^p-2(\delta_0+R(\xi))_+^p-k_1(R(\xi)-S(\xi))$ and $g=-c^2\nu_1\ddot{S}(\xi)-k_1(S(\xi)-R(\xi))$, where R and S constitute the solution obtained from the iterations of scheme III, then f and g are generally close to zero. This confirms that the schemes using Fourier analysis and the convolution theorem actually provide solutions satisfying, up to a small residual (presumably created by the discretization), equations (7) and (8).

We subsequently tried solving equations (7) and (8) using Newton's method, utilizing the solution from scheme III as a good initial seed for our iterations and as a means for obtaining information about boundary conditions; i.e., this approach side-steps both concerns originally present in the context of the direct method of scheme I. As indicated by the above residuals, while the initial guess does not directly solve our system to the prescribed accuracy, it is found to be close enough that the Newton's method will generically, within our computations, retain the relevant profile, rapidly converging to a solution of scheme I, as shown in figure 2.

Importantly, we have tested that 'distilling' this solution and its time derivative on the lattice (i.e., returning from the variable ξ to the integer index n), we retrieve genuinely traveling solutions of the original system of differential equations.

The above schemes provide us with a solution of the strain formulation problem for $R(\xi)$ and $S(\xi)$. However, an intriguing question concerns the reconstruction on the basis of these fields of the corresponding displacement ones r and s since $R(\xi)=r(\xi-1)-r(\xi)$ and $S(\xi)=s(\xi-1)-s(\xi)$. Assuming that we know $r(\xi_0)$, then $r(\xi_0-k)=r(\xi_0)+R(\xi_0-1)+R(\xi_0-2)+\ldots+R(\xi_0-k)$. So in order to fully restore r and s, we have to know their values in an interval of length 1. Assuming r and s are zero around the right end of the domain, we restored r and s from R and S in figure 2, confirming that they indeed solve equations (5)and (6). However, given this 'ambiguity' in the reconstruction, it should be noted that r and s obtained in figure 2 are not the only possible solution pair. In fact, using functions different from the solution of schemes II or III as initial guesses is also possible for

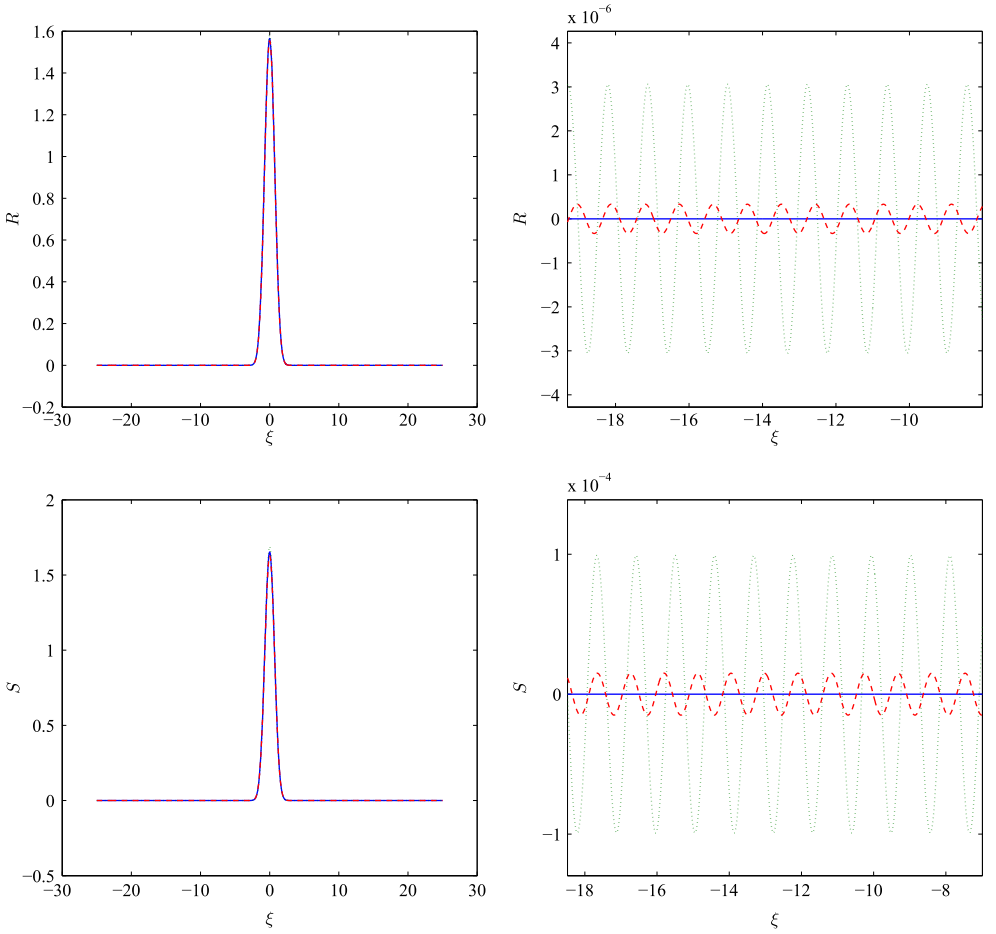

Figure 1. The top (resp. bottom) panels show the solutions for $R(\xi)$ (resp. $S(\xi)$) obtained from scheme III for $k_0 = 2\pi - 0.5$ (dashed line), 2π (solid line), $2\pi + 0.5$ (dotted line). The right panels are the corresponding zooms of the oscillating tails of the solutions in the left panels. Our computations indicate that when $k_0 \neq 2n\pi$ where $n \in \mathbb{Z}$, the oscillating tails are generically present. For these computations, $L = 30.16$ and $c = k_1 = 1$.

Table 1. Different situations we computed and their conditions

Case	Domain	Method	Tails of the solution
anti-resonance ($\frac{k_0}{2\pi} \in \mathbb{Z}$)	infinite domain $(-\infty, \infty)$	solved by scheme II	rapidly decaying tails
resonance ($\frac{k_0}{2\pi} \notin \mathbb{Z}$)	infinite domain $(-\infty, \infty)$	Fourier transform and scheme II fail	N/A
resonance ($\frac{k_0}{2\pi} \notin \mathbb{Z}$ and $k_0\frac{L}{\pi} \notin \mathbb{Z}$)	finite domain $[-L, L]$	singularities avoided, solved by scheme III	nondecaying oscillatory tails

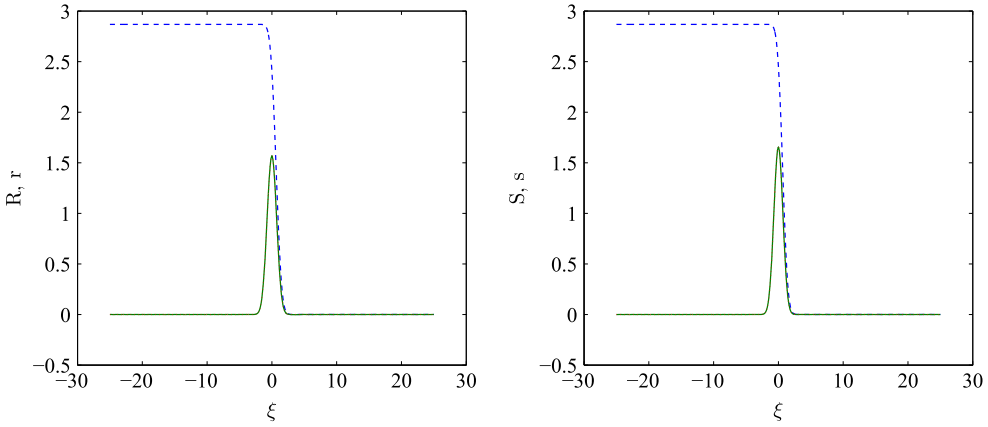

Figure 2. The left (right) panel showcases the solutions of R (S) from scheme I (solid line) and scheme III (dotted line) for $k_0 = 2\pi$ (these results are effectively identical). Also, the corresponding solution in the case of displacements r (s) by scheme I (dashed line) is obtained if we assume $r = s = 0$ at the right end of the domain. If we choose $k_0 \neq 2n\pi$, the plots will be similar except that all of these solutions will have oscillating tails. It can be seen that the solutions from schemes I and III are indistinguishable to the eye, which confirms the reliability of the Fourier approach. Here we set $L = 30.16$ in scheme III and $c = k_1 = 1$.

scheme I to converge to a solution. For example, the oscillating wave solutions illustrated in figure 3 can also solve equations (5) and (6). In fact, it has been directly checked that both the profiles of figure 2 and those of figure 3 when distilled on the lattice constitute genuine traveling waves of the original dynamical problem. Nevertheless, the latter waves are less relevant for our considerations from a physical perspective, as they do not constitute fronts at the displacement and pulses at the strain level.

Lastly, at the level of the present considerations it is relevant to point out that the identified solutions have been illustrated in figure 4 to exhibit genuine traveling with the prescribed speed (of $c = 1$). This is done for the anti-resonant case of $k_0 = 2\pi$ (associated with the waveform of figure 2) in the top panels. Here there is no discernible tail. It has also, however, been demonstrated in the bottom panels for the case of $k_0 = 2\pi - 0.5$. Here, as per figure 1, we expect the tails to be present, yet they are not observable in a linear scale due to their small amplitude. It is typically observed that the amplitude of the nanopteronic oscillation tails is several orders of magnitude smaller than that of the main pulse. Importantly, this feature has also been observed in the experiments of [62]. In fact, our numerical implementations of situations with different setups (including the setups for the experiments in [62]) via schemes I or III also corroborated this feature. For this reason, we have used a logarithmic scale in the bottom panels of figure 4, which can clearly showcase the nontrivial traveling oscillatory tails.

3.3. Study of parameters k_1 and ν_1

Having illustrated how to obtain solutions which are equivalent between schemes II and III, and how to utilize these to also obtain a direct solution from scheme I, we now turn to the examination of parametric variations within these schemes. The canonical parameters whose variations we consider are the linear coupling with the local resonator k_1, as well as the

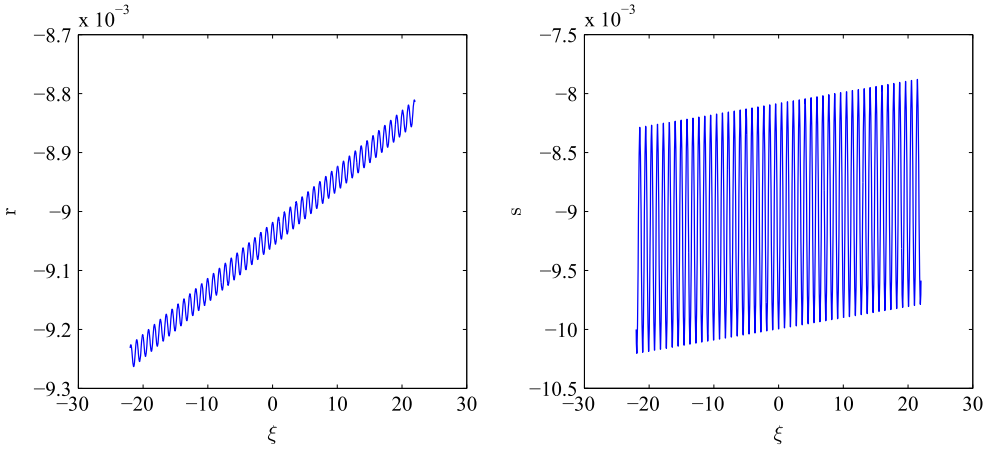

Figure 3. The left (right) panel shows another possible, yet less physically interesting, solution of r (s) obtained from scheme I. Here we set $c = k_1 = 1$, $k_0 = 2\pi + 0.6$.

effective mass ν_1 of the resonator. We also note in passing that c will also be allowed to change and the effects of such a variation will be discussed in this section. However, the remark in section 2.1 and the relationship between these parameters imply that study of two parameters will be essentially sufficient to capture the full picture and that the variation of the third one can be indirectly inferred from them.

When k_0 is a multiple of 2π and gets fixed, consideration of $m_1(\xi)$ proves rather insightful towards understanding the effects of the parameters k_1 and ν_1, since the properties of the solution of equation (14) are determined by those of the kernel $m_1(\xi)$. If ν_1 is fixed and k_1 and c vary to retain the same value of k_0, m_1 will only change in overall amplitude and a family of solutions differing in amplitudes and speeds will be obtained, as we mentioned above in section 2.1. Suppose we fix k_1 and change ν_1 and c, the shape and the properties of m_1 can change significantly. When $c \geqslant \sqrt{\frac{k_1(1+k_0)}{k_0^2}}$, $m_1(\xi)$ is increasing on $(-\infty, 0)$ (hence decreasing on $(0, \infty)$) and always non-negative. There also exists $c_0 \in (0, \sqrt{\frac{k_1(1+k_0)}{k_0^2}})$ such that $m_1(\xi)$ is non-negative on $(-\infty, \infty)$ if and only if $c \geqslant c_0$. Though not necessary, being non-negative and increasing on $(-\infty, 0)$ are properties of the kernel that in our numerical computations appear to facilitate the convergence of scheme II towards a solution. If k_1 and ν_1 vary at the same time and c remains unchanged, it is equivalent to considering the previous two cases together and we do not include the corresponding details here.

If we choose $k_0 \neq 2n\pi$ but still assign it a constant value, we will discuss the effects of ν_1 and k_1 on the solution of R based on $\tilde{m}_1$ and $\tilde{M}_{1_k}$ rather than m_1 since scheme II becomes inapplicable in this case. Though the period of the oscillating tails is always $\frac{2\pi}{k_0}$ since k_0 is fixed, the amplitude of the tails can be very sensitive to other parameters. First, only changing k_1 and c to keep the value of k_0 fixed can generate a family of solutions with same shape but different amplitudes, just as described in the remark of section 2.1. When c is fixed and k_1 and ν_1 vary, $\tilde{M}_{1_k} = \frac{1}{c^2}(1 - k_1 \frac{1}{c^2(k_0^2 - (k\frac{\pi}{L})^2)})\mathrm{sinc}^2(k\frac{\pi}{L})$ is either always increasing or always decreasing over k_1 for any integer k. Moreover, $\max_\xi |\tilde{m}_1(\xi)|$, or $\tilde{m}_1(0) = \sum_{k=-\infty}^{\infty} \tilde{M}_{1_k} = \sum_{k=-\infty}^{\infty} \frac{1}{c^2}\mathrm{sinc}^2(k\frac{\pi}{L})$

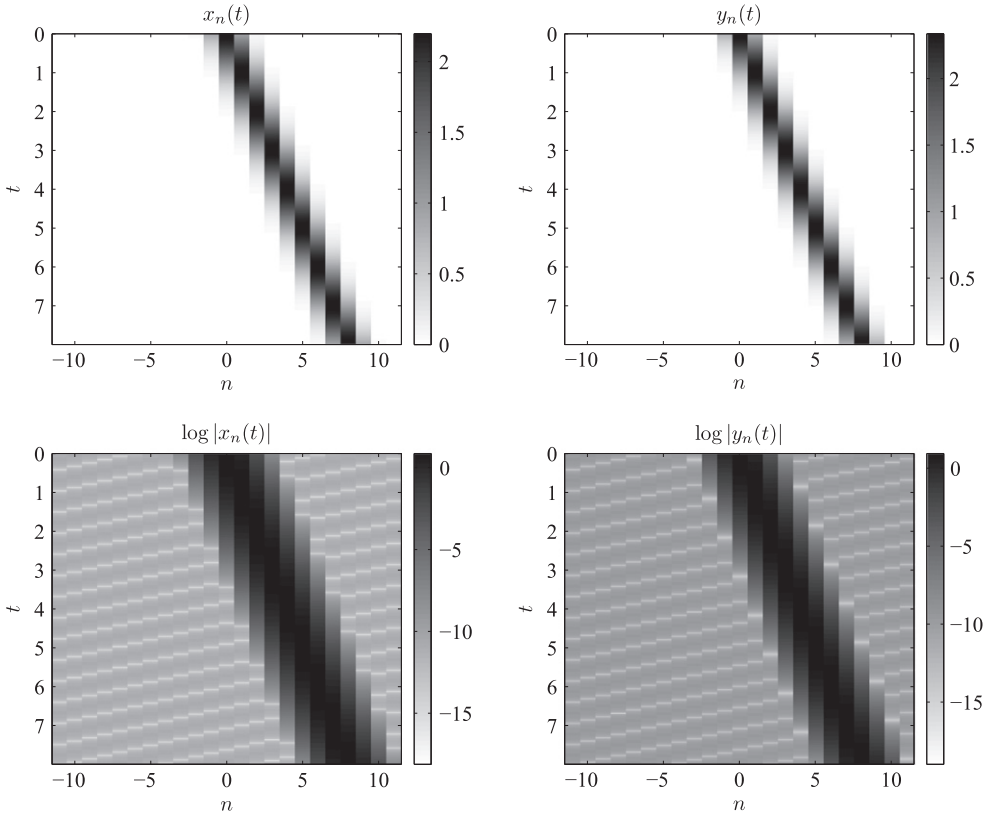

Figure 4. The top panels show the space–time evolution of the traveling wave solution of x_n and y_n to equations (9) and (10) for the anti-resonance case $k_0 = 2\pi$ from scheme I, namely Newton's method with initial guess from scheme III. The bottom panels illustrate the corresponding space–time evolutions on a logarithmic scale for the case $k_0 = 2\pi - 0.5$. Here, it can be clearly seen that the oscillation persists in the background. In these figures, we have set $c = 1$ and $k_1 = 7$.

$-\,k_1\sum_{k=-\infty}^{\infty}\frac{1}{c^4(k_0^2-(k\frac{\pi}{L})^2)}\mathrm{sinc}^2(k\frac{\pi}{L})$, always grows (or decays) as k_1 increases. Again, the case of varying c and ν_1 is just the composition of the previous two cases.

In the discussion above, we assumed k_0 as a constant parameter while other parameters were varied to maintain the constant value of k_0. In the following discussion of this subsection, we will allow k_0 to vary and change other parameters freely. If we fix c and k_1 and only allow the changing of ν_1, we find that $\tilde{M}_{1_k} = \frac{1}{c^2}(1 - \frac{k_1}{k_1(1+1/\nu_1)-(ck\frac{\pi}{L})^2})\mathrm{sinc}^2(k\frac{\pi}{L})$ for any integer k (hence $\tilde{m}_1(0)$) will decrease as ν_1 increases from $\frac{k_1}{(\frac{n\pi}{cL})^2-k_1}$ to $\frac{k_1}{(\frac{(n+1)\pi}{cL})^2-k_1}$ for any $n \in \mathbb{Z}$. Similarly, we can show that $\tilde{M}_{1_k}$ increases as k_1 increases from $\frac{1}{(1+1/\nu_1)}(\frac{n\pi}{Lc})^2$ to $\frac{1}{(1+1/\nu_1)}(\frac{(n+1)\pi}{Lc})^2$ or c^2 decreases from $(1 + 1/\nu_1)k_1(\frac{L}{n\pi})^2$ to $(1 + 1/\nu_1)k_1(\frac{L}{(n+1)\pi})^2$. These strict monotone properties of $\tilde{m}_1$ are revealed in figure 5. The figure also illustrates the smooth behavior of $\bar{m}_i$ versus the singular (at the resonance points) behavor of $\tilde{m}_1$ in the tails and how these two functions become identical at $k_0\frac{L}{\pi} + \frac{1}{2} \in \mathbb{Z}$.

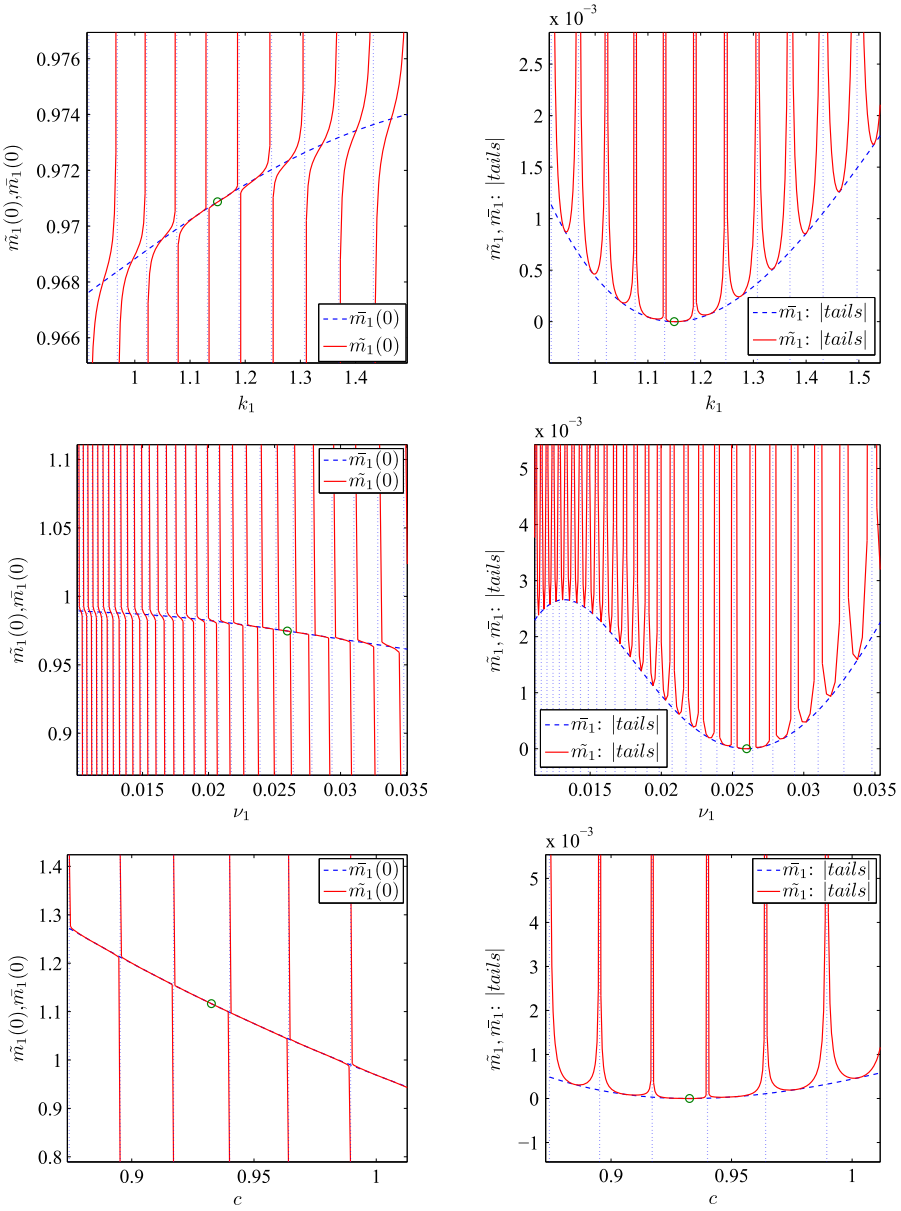

Figure 5. The top left panel shows how $\tilde{m}_1(0)$ (solid line) and $\bar{m}_1(0)$ (dashed line) change over k_1 and the top right panel shows the change of the amplitude of oscillating tails of $\tilde{m}_1$ (solid line) and $\bar{m}_1$ (dashed line) as k_1 grows. The middle and bottom panels follow the same structure as the top row but reveal the results when varying ν_1 and c, respectively. The figures show that $\tilde{m}_1$ blows up every time $k_0\frac{L}{\pi} \in \mathbb{Z}$ but $\tilde{m}_1(0)$ features strictly increasing or decreasing trend between these singularity points (where parameters satisfy $k_0\frac{L}{\pi} \in \mathbb{Z}$). It should be noted that the dotted vertical lines indicate the singularity points and are added just to better illustrate the boundaries of each interval. These figures also show $\tilde{m}_1$ intersects with $\bar{m}_1$ when $k_0\frac{L}{\pi} + \frac{1}{2} \in \mathbb{Z}$ or $k_0 = 2n\pi$ and especially at $k_0 = 2n\pi$ the kernel $\tilde{m}_1$ loses its oscillating tails (marked by green circles in the right panels). In these computations we set $c = 1$, $k_1 = 1$ and $\nu_1 = 0.03$ when they are constants.

Due to the nature of the convolution equation $R(\xi) = (m^*(R)_+^{3/2})(\xi) = \int_{-L}^{L} m(y)(R(\xi - y))_+^{3/2}\mathrm{d}y$ with m standing for $\tilde{m}_i$ or $\bar{m}_i$, changes in the kernel m will be translated into ones for the solution R, as will be explained heuristically below. Based on our knowledge of m and R, we know they are symmetric functions and (arbitrarily splitting them into a core and tail segment) they can be written as

$$m(\xi) = m_I(\xi) + m_O(\xi) \coloneqq m(\xi)I_{[-L_1,L_1]}(\xi) + m(\xi)I_{(-L,-L_1)\cup(L_1,L)}(\xi), \quad (23)$$

$$R(\xi) = R_I(\xi) + R_O(\xi) \coloneqq R(\xi)I_{[-L_2,L_2]}(\xi) + R(\xi)I_{(-L,-L_2)\cup(L_2,L)}(\xi) \quad (24)$$

with $m_I(-L_1) = m_I(L_1) = R_I(-L_2) = R_I(L_2) = 0$. Then the convolution equation can be considered as the sum of 4 parts $R(\xi) = \int_{-L}^{L} m(y)(R(\xi - y))_+^{3/2}\mathrm{d}y = A + B + C + D$, where $A \coloneqq \int_{-L_1}^{L_1} m_I(y)(R_I(\xi - y))_+^{3/2}\mathrm{d}y$, $B \coloneqq \int_{-L_1}^{L_1} m_I(y)(R_O(\xi - y))_+^{3/2}\mathrm{d}y$, $C \coloneqq \int_{\xi-L_2}^{\xi+L_2} m_O(y)(R_I(\xi - y))_+^{3/2}\mathrm{d}y$ and $D \coloneqq \int_{-L}^{L} m_O(y)(R_O(\xi - y))_+^{3/2}\mathrm{d}y$. If we only focus on the cases relevant to our numerical results, we will also assume $\frac{\max_\xi |R_I(\xi)|}{\max_\xi |R_O(\xi)|} \gg \frac{\max_\xi |m_I(\xi)|}{\max_\xi |m_O(\xi)|} \gg \frac{L}{L_1} > \frac{L}{L_2}$.

With all these conditions, it can be shown that the maximum of the solution $\max_\xi |R(\xi)| = R(0) = \int_{-L}^{L} m(y)(R(y))_+^{3/2}\mathrm{d}y = A + B + C + D \approx A = \int_{-L_1}^{L_1} m_I(y)(R_I(y))_+^{3/2}\mathrm{d}y$. As a result, when m_O is changed to $m_{O,\mathrm{new}} = qm_O$ (assuming $q = O(1)$ or q such that m_{new} and I_{new} still satisfy our conditions) and m_I is fixed, the maximum of the solution R_{new} (namely $R_{\mathrm{new}}(0)$) will almost remain at its (previous) value $R(0)$. While if $m_{I,\mathrm{new}} = qm_I$ and m_O is unchanged, $R_{I,\mathrm{new}}$ will be close to $\frac{1}{q^2}R_I$ thus $R_{\mathrm{new}}(0) \approx \frac{1}{q^2}R(0)$. Suppose ξ_0 satisfies $R_O(\xi_0) = \max_\xi |R_O(\xi)|$ and $L > |\xi_0| > L_1 + L_2$, then the amplitude of the tails $R(\xi_0) = A + B + C + D = B + C + D \approx C = \int_{\xi-L_2}^{\xi+L_2} m_O(y)(R_I(\xi - y))_+^{3/2}\mathrm{d}y$ because A becomes 0 and C is dominant over the remaining contributions. By arguments similar to the above, $m_{O,\mathrm{new}} = qm_O$ and $m_{I,\mathrm{new}} = m_I$ will imply $R_{\mathrm{new}}(\xi_0) \approx qR(\xi_0)$. If $m_{O,\mathrm{new}} = m_O$ and $m_{I,\mathrm{new}} = qm_I$, then $R_{\mathrm{new}}(\xi_0) \approx \frac{1}{q^3}R_{\mathrm{new}}(\xi_0)$ since $R_{I,\mathrm{new}}(\xi) \approx \frac{1}{q^3}R_I$.

Although the effects of parametric variations on the kernel m, which include changing the shape of $m_I(\xi)$ and the period of $m_O(\xi)$, are much more complicated than merely introducing multiplicative factors on center or tails, the properties above can still be helpful towards predicting the changes of R and they are straightforward to apply. As figure 6 shows, when ν_1 varies in a chosen range and $\tilde{m}_1(0)$ changes slowly, the tails of $\tilde{m}_1$ reflect the form of the corresponding tails of R very well. At the same time, it should be noticed that $R(0)$ seems not very sensitive about the points $\frac{k_0 L}{\pi} \in \mathbb{Z}$ even though $\tilde{m}_1(0)$ blows up quickly when approaching those points.

4. Conclusions and future challenges

In the present work, we have revisited a topic of intense current theoretical, numerical and experimental investigation, namely the formation of weakly nonlocal traveling waves in granular chains with local resonators. We attempted to provide a systematic insight on the different possible numerical methods that can be used to identify such traveling waves. Additionally, we highlighted the different challenges that each of these methods may encounter. In total, we analyzed three methods. The first consisted of a direct solution of the co-traveling wave boundary value problem for the associated differential advance-delay equation. The second involved the Fourier representation of this problem and considered an

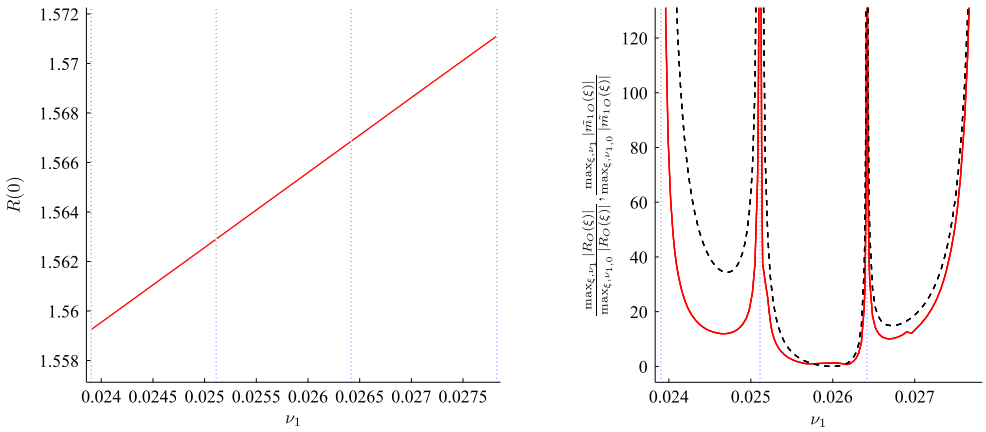

Figure 6. The left panel shows the changing of amplitude of R (or $R(0)$) as k_1 grows while the right panel reveals the agreement between the changing of tails of R and that of tails of $\tilde{m}_1$. In the latter panel, the solid red line is for $\frac{\max_{\xi,\nu 1} \mid R_O(\xi) \mid}{\max_{\xi,\nu 1,0} \mid R_O(\xi) \mid}$ as ν_1 changes and the changing $\frac{\max_{\xi,\nu 1} \mid \tilde{m}_{1O}(\xi) \mid}{\max_{\xi,\nu 1,0} \mid \tilde{m}_{1O}(\xi) \mid}$ is described by the black dashed line. Here $\nu_{1,0} = 0.025\,75$, $c = 1$ and $k_1 = 1$ are the parameters we used in the computation.

inverse Fourier transform of the problem to provide an alternative formulation of the real space problem. This idea was carried out using Fourier transforms defined on the infinite domain. Finally, the third one considered the Fourier series version of the second method to extend it to more (and indeed rather generic) situations. The difficulties existing in each case were identified and explored, including the limitations of the Fourier transform (which is restricted to the anti-resonance case) and of the Fourier series, the need for a suitable initial guess for the first method and the boundary conditions thereof, as well as the issue of converting the strain into a displacement formulation. We explored how the use of finite domains under generic non-resonance conditions may enable the convergence of the third scheme (and how the anti-resonance enables the convergence of the second scheme to a similar solution). We then used good initial guesses from these schemes to lead to convergent solutions of the first scheme and were able to reconstruct based on that also the corresponding displacement profiles. An interesting byproduct of the parametric variations considered was the ability to identify anti-resonance parameter values for which the generic existence of tails (in our weakly nonlocal solitary waves) was annulled, enabling the identification of regular, rapidly decaying (on each side) solitary waves.

While we believe that the above analysis may shed a partial light on the identification of traveling solitary wave solutions, there remains a sizable number of open problems in this direction. Among the significant challenges posed by the experimental observations of [62] we note the following. For different parameter values than for the ones where the weakly nonlocal solutions were identified, it was found that a breathing while traveling behavior was possible. It would be extremely interesting to try to identify such breathing traveling waves and to explore the recurrence type of dynamics that appears to lead to their formation. Furthermore, in [62], the nature of experimental excitations led to the formation of single-sided (i.e., bearing tails on only one side) tails. Exploring the potential of such exact solutions is an interesting question in its own right. Another aspect that was briefly explored in [62] was the inclusion of a higher number of resonators. In the case of more resonators, the possibility

of steady (or even breathing) traveling waves was found to be less typical. Instead, it was found that decay of the original pattern's amplitude was the most commonly observed scenario. Identifying these cases from the dynamical systems/Fourier analysis perspective presented herein and more systematically examining the effect of corresponding parametric variations would constitute a particularly relevant task for future work.

Acknowledgments

P G K acknowledges support from the National Science Foundation under grant DMS-1312856, from ERC and FP7-People under grant 605096, from the US-AFOSR under grant FA9550-12-10332, and from the Binational (US-Israel) Science Foundation through grant 2010239. P G K's work at Los Alamos is supported in part by the US Department of Energy. AS is partially supported by NSF grant # 1313107. P G K also gratefully acknowledges discussions on this theme with G Theocharis and D J Frantzeskakis.

References

[1] Nesterenko V F 2001 *Dynamics of Heterogeneous Materials* (New York: Springer)
[2] Sen S, Hong J, Bang J, Avalos E and Doney R 2008 *Phys. Rep.* **462** 21–66
[3] Kevrekidis P G 2011 *IMA J. Appl. Math.* **76** 389–423
[4] Theocharis G, Boechler N and Daraio C 2013 *Phononic Crystals and Metamaterials* (New York: Springer) ch 6
[5] Daraio C, Nesterenko V F, Herbold E B and Jin S 2006 *Phys. Rev.* E **73** 026610
[6] Hong J 2005 *Phys. Rev. Lett.* **94** 108001
[7] Fraternali F, Porter M A and Daraio C 2010 *Mech. Adv. Mater. Struct.* **17** 1–19
[8] Doney R and Sen S 2006 *Phys. Rev. Lett.* **97** 155502
[9] Khatri D, Daraio C and Rizzo P 2008 *SPIE* **6934** 69340U
[10] Coste C and Gilles B 2008 *Phys. Rev.* E **77** 021302
[11] Daraio C, Nesterenko V F and Jin S 2004 *AIP Conf. Proc.* **706** 197–200
[12] Daraio C and Nesterenko V F 2006 *Phys. Rev.* E **73** 026612
[13] de Billy M 2000 *J. Acoust. Soc. Am.* **108** 1486–95
[14] de Billy M 2006 *Ultrasonics* **45** 127–32
[15] Gilles B and Coste C 2001 Nonlinear elasticity of a 2D regular array of beads *Powders and Grains 4th Int. Conf. on Micromechanics of Granular Media (Sendai)*
[16] Gilles B and Coste C 2003 *Phys. Rev. Lett.* **90** 174302
[17] Nesterenko V F 1983 *J. Appl. Mech. Tech. Phys.* **24** 733–43
[18] Porter M A, Daraio C, Herbold E B, Szelengowicz I and Kevrekidis P G 2008 *Phys. Rev.* E **77** 015601
[19] Porter M A, Daraio C, Szelengowicz I, Herbold E B and Kevrekidis P G 2009 *Physica* D **238** 666–76
[20] Rosas A and Lindenberg K 2004 *Phys. Rev.* E **69** 037601
[21] Shukla A 1991 *Opt. Lasers Eng.* **14** 165–84
[22] Molinari A and Daraio C 2009 *Phys. Rev.* E **80** 056602
[23] Herbold E B and Nesterenko V F 2007 *Shock Compression Condens. Matter* **955** 231–4
[24] Daraio C, Nesterenko V F, Herbold E B and Jin S 2006 *Phys. Rev. Lett.* **96** 058002
[25] Herbold E B and Nesterenko V F 2007 *Appl. Phys. Lett.* **90** 261902
[26] Hong J B and Xu A G 2002 *Appl. Phys. Lett.* **81** 4868–70
[27] Job S, Melo F, Sokolow A and Sen S 2005 *Phys. Rev. Lett.* **94** 178002
[28] Job S, Melo F, Sokolow A and Sen S 2007 *Granular Matter* **10** 13–20
[29] Melo F, Job S, Santibanez F and Tapia F 2006 *Phys. Rev.* E **73** 041305
[30] Boechler N, Theocharis G, Job S, Kevrekidis P G, Porter M A and Daraio C 2010 *Phys. Rev. Lett.* **104** 244302
[31] Job S, Santibanez F, Tapia F and Melo F 2009 *Phys. Rev.* E **80** 025602(R)

[32] Theocharis G, Kavousanakis M, Kevrekidis P G, Daraio C, Porter M A and Kevrekidis I G 2009 *Phys. Rev.* E **80** 066601
[33] Chong C, Li F, Yang J, Williams M O, Kevrekidis I G, Kevrekidis P G and Daraio C 2014 *Phys. Rev.* E **89** 032924
[34] Sen S and Mohan T R Krishna 2009 *Phys. Rev.* E **79** 036603
[35] Ávalos E and Sen S 2009 *Phys. Rev.* E **79** 046607
[36] Starosvetsky Y and Vakakis A F 2010 *Phys. Rev.* E **82** 026603
[37] Jayaprakash K R, Starosvetsky Y and Vakakis A F 2011 *Phys. Rev.* E **83** 036606
[38] Szelengowicz I, Hasan M A, Starosvetsky Y, Vakakis A and Daraio C 2013 *Phys. Rev.* E **87** 032204
[39] Stefanov A and Kevrekidis P G 2012 *J. Nonlinear. Sci.* **22** 327–49
[40] Stefanov A and Kevrekidis P G 2013 *Nonlinearity* **26** 539–64
[41] Chong C, Kevrekidis P G and Schneider G 2014 *Discrete Continuous Dyn. Syst.* A **34** 3403–18
[42] Leonard A, Chong C, Kevrekidis P G and Daraio C 2014 *Granular Matter* **16** 531–42
[43] English J M and Pego R L 2005 *Proc. AMS* **133** 1763–8
[44] Chatterjee A 1998 *Phys. Rev.* E **59** 5912–9
[45] Ahnert K and Pikovsky A 2009 *Phys. Rev.* E **79** 026209
[46] Spadoni A and Daraio C 2010 *PNAS* **107** 7230
[47] Liang B, Yuan B and Cheng J C 2009 *Phys. Rev. Lett.* **103** 104301
[48] Li X-F, Ni X, Feng L, Lu M-H, He C and Chen Y-F 2011 *Phys. Rev. Lett* **106** 084301
[49] Boechler N, Theocharis G and Daraio C 2011 *Nat. Mater.* **10** 665–8
[50] Li F, Anzel P, Yang J, Kevrekidis P G and Daraio C 2014 **5** 5311
[51] Daraio C, Nesterenko V F, Herbold E B and Jin S 2005 *Phys. Rev.* E **72** 016603
[52] Nesterenko V F, Daraio C, Herbold E B and Jin S 2005 *Phys. Rev. Lett.* **95** 158702
[53] Yang J, Sangiorgio S, Borkowski S, Silvestro L, Nardo D, Daraio C and Ebramzadeh E 2012 *J. Biomed. Eng.* **134** 101001
[54] Ni X, Rizzo P, Yang J, Khatri D and Daraio C 2012 *NDT & E Int.* **52** 76–85
[55] MacKay R S 1999 *Phys. Lett. A* **251** 191–2
[56] Friesecke G and Wattis J A D 1994 *Commun. Math. Phys.* **161** 391–418
[57] James G 2011 *Math. Mod. Meth. Appl. Asci* **21** 2335
[58] James G, Kevrekidis P G and Cuevas J 2013 *Physica* D **251** 39
[59] Bonanomi L, Theocharis G and Daraio C 2015 *Phys. Rev.* E **91** 033208
[60] Gantzounis G, Serra-Garcia M, Homma K, Mendoza J M and Daraio C 2013 *J. Appl. Phys.* **114** 093514
[61] Kevrekidis P G, Vainchtein A, Serra Garcia M and Daraio C 2013 *Phys. Rev.* E **87** 042911
[62] Kim E, Li F, Chong C, Theocharis G, Yang J and Kevrekidis P G 2015 *Phys. Rev. Lett.* **114** 118002
[63] Remoissenet M 1999 *Waves Called Solitons* (Berlin: Springer)
[64] Boyd J 1998 *Weakly Nonlocal Solitary Waves and Beyond-All-Orders Asymptotics* (Amsterdam: Kluwer)
[65] Hochstrasser D, Mertens F G and Büttner H 1989 *Physica* D **35** 259